

Stacking order effects on the energetic stability and electronic properties of n -doped graphene/h-BN van der Waals heterostructures on SiC(0001)

D. P. de Andrade Deus,^{1,*} J. M. J. Lopes,² and Roberto H. Miwa^{3,†}

¹*Instituto Federal de Educação, Ciência e Tecnologia do Triângulo Mineiro, Uberaba, C. P. 1020, 38064-190, Minas Gerais, Brazil*

²*Paul-Drude-Institut für Festkörperelektronik, Leibniz-Institut im Forschungsverbund Berlin e.V., 10117 Berlin, Germany*

³*Instituto de Física, Universidade Federal de Uberlândia, C.P. 593, 38400-902, Uberlândia, MG, Brazil*

(Dated: March 16, 2023)

ABSTRACT

Heterostructures based on the stacking of two-dimensional materials with different electronic properties have been the subject of several studies addressing the development of novel devices with multiple functionalities. Among them, van der Waals (vdW) systems composed of graphene (G) and hexagonal boron nitride (h-BN) have been extensively investigated, including recent experimental studies on the large-scale synthesis of h-BN on graphene/SiC(0001) templates. Interestingly, their results suggest that besides vdW epitaxy of h-BN on graphene, confined growth of h-BN monolayers between graphene and SiC(0001) could also take place, leading to h-BN encapsulation. In this work, we have performed a theoretical study, based on first-principles calculations, of G/h-BN heterostructures on SiC(0001), the latter covered by a carbon buffer layer (SiC). Our findings reveal that, indeed, there is an energetic preference for the encapsulation of h-BN below a single layer of graphene on SiC, viz.: G/h-BN/SiC in the case of bilayer systems and G/h-BN/G/SiC in the case of trilayer systems. Electronic structure calculations show that the linear energy band dispersion of graphene is preserved in the bilayer systems independent of the stacking order, however, with the Dirac points lying in different energy positions due to the different electron doping level of graphene. In the trilayer systems, the n -type doping level of graphene also depends on the stacking order. The electronic band structure of G/h-BN/G/SiC is characterized by two Dirac points, both below the Fermi level, but with different energies, while the other (energetically less stable) systems, G/G/h-BN/ and h-BN/G/G/SiC are characterized by the emergence of parabolic bands near the Fermi level. Additional structural characterizations of these G/h-BN heterostructures on SiC were carried out based on simulations of C-1s core-level-shift (CLS) and carbon K-edge X-ray absorption near edge spectroscopy (XANES), with the goal of assisting future experimental spectroscopy in these graphene/h-BN vdW systems.

I. INTRODUCTION

Van der Waals (vdW) heterostructures combining different two-dimensional (2D) materials are very promising for the realization of atomically thin devices with tailored properties and functionalities[1]. No matter what combination of 2D crystals is desired, their fabrication is usually achieved via sequential stacking of individual flakes exfoliated from bulk crystals [1, 2]. Although this method allows for preparing samples and devices with a high degree of perfection and quality, the small lateral size (tens of μm) of the produced material is unsuitable for applications. Moreover, interface contamination introduced during heterostructure assembly [3, 4] may deteriorate the resulting properties.

A promising alternative to such method is to realize the large-scale synthesis of 2D materials on top of each other via vdW epitaxy [5], utilizing either physical- or chemical-vapour deposition methods. Nevertheless, the controlled realization of single crystalline heterostructures via vdW epitaxy is challenging due to additional effects that may take place besides vdW growth. For example, the existence of surface defects such as grain

boundaries and nanoholes results in the intercalation of adatom species underneath the 2D template, which may lead to the formation of another material (2D or 3D) at the interface between the 2D template and the host substrate. Feldberg et al.[6] reported on the spontaneous intercalation of Ga species during growth of GaN on epitaxial graphene on SiC(0001) via molecular beam epitaxy (MBE). Specifically, they observed the formation of an ordered Ga bilayer between the carbon buffer layer and SiC(0001). Similarly, the results from Heilmann et al. [7] for MBE growth of h-BN on epitaxial graphene/SiC(0001) suggests that adatom intercalation below graphene takes place. This result is in agreement with their most recent study [8], in which epitaxial graphene [on SiC(0001)] having a defect patterning produced by He ions was utilized as a growth template for h-BN. In this case, besides the nucleation (and lateral growth) of insulating h-BN monolayer islands on the surface (as unambiguously confirmed by conductive atomic force microscopy), the single-layer graphene regions also exhibited a roughened and somewhat wrinkled surface morphology that was however still conductive, as expected for graphene. This suggests that the growth of another material, possibly boron nitride, took place

below single-layer graphene, mostly likely due to the B and N intercalation. It is worth noting that intercalation has also been observed during epitaxial growth of h-BN/graphene heterostructures on metals.[9, 10]

If, on the one hand, intercalation during vdW epitaxy is unwanted, it also represents a very promising path for the controlled synthesis of novel material systems. In fact, Al Balushi et al. [11] developed an experimental scheme that enhanced the intercalation of Ga and N species below epitaxial graphene on SiC(0001), which allowed for the realization of a 2D-like GaN phase encapsulated between graphene and SiC(0001). This approach has recently been generalized for achieving confined epitaxy of 2D metals as well as oxides at the interface between graphene and SiC(0001) [12, 13]. It could in principle also be implemented to controllably create an atomically thin h-BN below epitaxial graphene, which could lead to the electronic decoupling of graphene from the buffer layer/SiC(0001).

Considering the reported facts, we performed a theoretical study, based on first-principles calculations, of the energetic stability and the structural and electronic properties of h-BN/graphene heterostructures on SiC(0001). Our findings confirm that 2D heterostructures where h-BN is encapsulated between graphene and buffer layer/SiC, or two graphene layers (i.e. graphene/h-BN/graphene on buffer layer/SiC), are energetically favorable when we consider bilayer (BL) and trilayer (TL) systems, respectively. Further calculations revealed that the graphene/h-BN stacking order on SiC(0001) can be characterized by different fingerprints on the electronic band structure and net charge transfer (i.e. electron and hole doping) profiles through the heterostructure. Finally, we have performed a set of spectroscopic simulations, carbon K-edge X-ray absorption near edge structure (XANES), and C-1s core-level-shift (CLS) in order to provide structural information about these stacked layers combined with the local electronic properties.

II. COMPUTATIONAL DETAILS

A. Structural optimizations, total energies, and electronic properties

Our DFT calculations were performed within the Perdew-Burke-Ernzerhof generalized gradient approximation [14], using the projector augmented wave (PAW) potentials,[15] as implemented in the Vienna Ab-initio Simulation Package(VASP) [16, 17]. The structural optimizations were done, including van der Waals corrections (vdW)[18] until the forces on each atom were smaller than 0.01 eV/Å and total energies converged within a 1×10^{-6} eV criterion. The Kohn-Sham (KS) wave functions were expanded in a plane-wave basis set with an energy cutoff (E_{cut}) of 600 eV. The sampling of the Brillouin-zone (BZ) was performed by using the Monkhorst-Pack (MP)[19] scheme with k-point meshes

of $5 \times 5 \times 1$ and $10 \times 10 \times 1$ for structural optimization and electronic properties, respectively.

A supercell possessing a periodicity of $(2\sqrt{3} \times 2\sqrt{3})R30^\circ$ is considered to simulate the interface that is formed by G/h-BN layers and SiC(0001) covered by a carbon buffer layer (SiC). The SiC(0001) surface was described by using a slab with three SiC bilayers and a vacuum region of 16 Å. Furthermore, we employ a supercell rotation method, in which graphene and h-BN sheets are rotated by 6.58° (23.4°) with respect to the direction of the armchair (zigzag) in relation to the substrate. By this method, the degree of mismatch between h-BN, graphene monolayer and bilayers is reduced to 0.4%. This model has been successfully applied in graphene bilayers and graphene/SiC interfaces[20–22]. As in these systems, it is expected that the weak van der Waals interaction, primarily responsible for the bonding between these systems, such a rotation does not induce any relevant perturbations in the electronic structure of the interface due to the aforementioned rotation.

B. XANES and CLS

The carbon K-edge X-ray absorption near-edge structure (XANES) and C-1s core-level shift (CLS) were simulated by using the X-spectra package[23–25] implemented in the Quantum-ESPRESSO (QE) code[26]. The KS orbitals were expanded in a plane-wave basis set with E_{cut} of 48 and 192 Ry for the single-particle wavefunction and total charge density, respectively, and MP $10 \times 10 \times 1$ k-points for the BZ sampling. For the carbon K-edge XANES, the initial state corresponds to a C-1s orbital ($|1s\rangle$) originating from the absorbing atom without a core-hole. This orbital is extracted by using the Gauge-Including Projector Augmented-Wave (GIPAW) method[27] to calculate the dipolar cross-section,

$$\sigma(\omega) \propto \omega \sum_n |\langle n | \hat{\mathbf{e}} \cdot \mathbf{r} | 1s \rangle|^2 \delta(\varepsilon_n - \varepsilon_{1s} - \hbar\omega). \quad (1)$$

The final state ($|n\rangle$) is obtained through the self-consistent solution of the KS equations for the whole system taking into account the core-hole effects in the pseudopotential of the (X-ray) absorbing atom[24]; $\hat{\mathbf{e}}$ indicates the polarization vector of the incident X-ray, and ε_n (ε_{1s}) is the energy of the final, $|n\rangle$ (initial, $|1s\rangle$) single-particle energy.

The CLS was obtained by using the so-called Δ SCF (Difference in Self-Consistent Field) approach [28, 29], where the core-level binding energy (BE) can be written as,

$$\text{BE} = E^{(n-1)} - E^{(n)}. \quad (2)$$

In this approach, $E^{(n-1)}$ and $E^{(n)}$ are the total energies of the ionized system with $(n-1)$ electrons (a core-hole), and of the ground system with n electrons, respectively. The former energy was obtained by using a

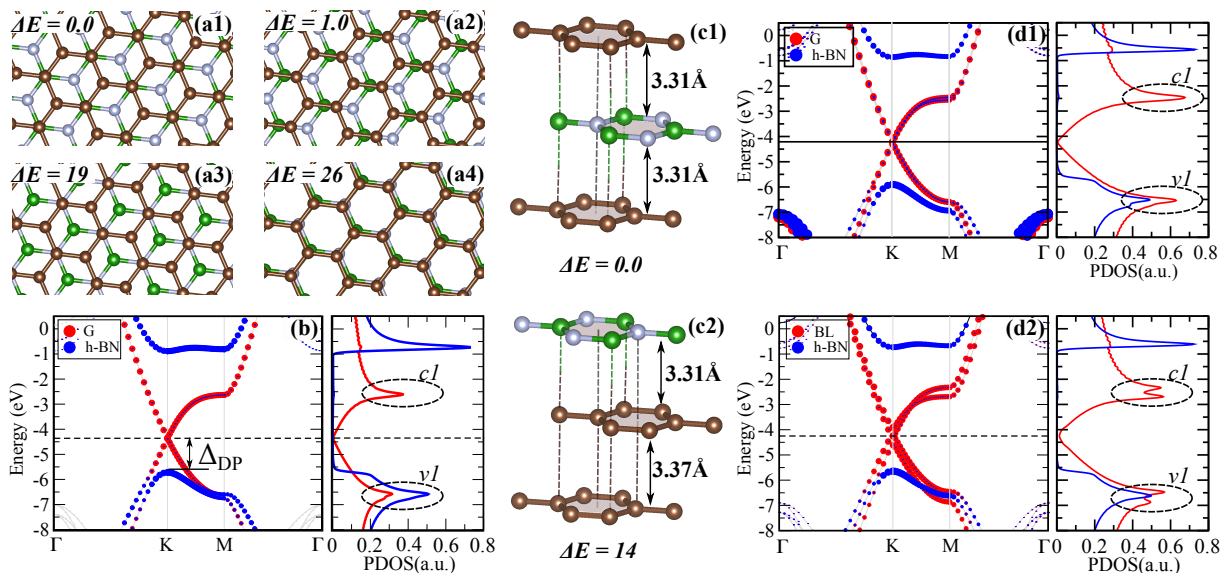


FIG. 1. Structural models of G/h-BN interface, Bernal stacking with the boron atom aligned with the carbon atom (a1), boron-nitrogen bonding aligned with the carbon atom (a2), Bernal stacking with the nitrogen atom aligned with the carbon atom (a3), eclipsed stacking (a4), and the total energy differences [ΔE in meV/(1×1)] with respect to the most stable configuration [(a1)]. (b) Electronic band structure, and projected density of states (PDOS) of the G/h-BN bilayer (a1). Structural models of the trilayer systems, G/h-BN/G with (c1), h-BN/G/G (c2) with the boron atom aligned with the carbon atom, and ΔE indicate the total energy difference [in meV/(1×1)] with respect to the most stable configuration [(c1)]. Electronic band structure, and PDOS of the trilayer systems, G/h-BN/G (d1) and h-BN/G/G (d2) The zero energy is set at the vacuum level, and the carbon, boron, and nitrogen atoms are represented by brown, green and white spheres.

pseudopotential generated based on the core-excited configuration of the atom [30]. Following the steps outlined in Refs. [31–33], we calculated $E^{(n)}$ using a regular pseudopotential (i.e., with no core-hole) and $E^{(n-1)}$ using a pseudopotential that included a core-hole in the investigated nonequivalent graphene carbon atoms. The same calculations were performed for a reference system, here a CH_4 molecule, resulting in BE_0 for the molecule’s carbon atom. The difference between BE and BE_0 results in the C-1s core-level-shift,

$$\Delta \text{BE} = \text{BE} - \text{BE}_0. \quad (3)$$

It is important to note that the molecule (reference system) is placed in the supercells in such a way that it does not interact with the SiC slab. Finally, the comparison with the experimental results can be done by adding the measured binding energy of the reference system (BE_0^{exp}), namely $\Delta \text{BE} + \text{BE}_0^{\text{exp}}$. For instance, using the measured binding energy of C-1s of the CH_4 molecule, $\text{BE}_0^{\text{exp}} = 283.5 \text{ eV}$ [34], we obtained a graphene’s C-1s core level BE of 284.07 eV, which is in good agreement with experimental results for (quasi-free standing) graphene monolayer on SiC [35].

III. RESULTS AND DISCUSSIONS

A. Free-standing bilayers and trilayers

We start our investigation by looking at the energetically most stable stacking geometry of the free-standing G/h-BN BL. The interface pattern characterized by Bernal (AB) stacking with the boron atom aligned with the carbon atom [Fig. 1(a1)], hereinafter referred to as G/h-BN, was found to be the most stable among the interfaces presented in Figs. 1(a1)–(a4) [36–38]. At the equilibrium geometry, we find an interlayer distance of 3.32 Å. Our total charge density results reveal the absence of chemical bonds between the graphene and h-BN layers; the G/h-BN binding strength is dictated by vdW long-range dispersive forces and no net charge transfer takes place between layers. In Fig. 1(b) we present the orbital projected electronic band structure of G/h-BN, characterized by (i) the Dirac bands of graphene lying within the energy gap of monolayer (ML) h-BN, with the Dirac point (DP) at 1.38 eV above the valence band maximum (at the K-point) of h-BN, $\Delta_{\text{DP}} = 1.38 \text{ eV}$, and (ii) the emergence of a (small) energy gap of 35 meV at the DP due to the graphene interaction with the h-BN layer [39, 40]. The electronic density of states (DOS), projected on the p_z orbitals, indicates the formation of Van Hove singularities (VHSs) in G/h-BN [41], labelled as $v1$ and $c1$ at -2.2 and 1.7 eV with respect to the Fermi level (E_F). It is worth noting that the electronic states at the

M-point govern these VHSs, where $v1$ is the result of interlayer $C-p_z+B-p_z$ hybridization and $c1$ is solely due to $C-p_z$ orbitals.

We next examined the structural model of TL systems composed of an h-BN ML encapsulated by graphene sheets (G/h-BN/G), and on top of graphene bilayer (h-BN/G/G). We have considered the Bernal stacking with the carbon atoms aligned with the boron atoms, and nitrogen atoms. We found that G/h-BN/G with the boron atoms aligned with the graphene carbon atom [Fig. 1(c1)] as the energetically most stable configuration[42], followed by the h-BN/G/G also with the boron-carbon alignment, Fig. 1(c2). The other G/h-BN/G and h-BN/G/G configurations, with the carbon atom immediately above(or below) the nitrogen atom, are less stable by 16 and 34 meV/(1×1). At the equilibrium geometry, the interlayer distances are practically identical to those found in G/h-BN. We have checked and confirmed these results by using other vdW approaches, Appendix-subsection A.

The electronic band structure and the DOS projected on the p_z orbitals of the G/h-BN/G TL, Fig. 1(d1), resemble those of the G/h-BN BL. This is evidenced by the preservation of the linear dispersion at the K-point, followed by an energy gap of 8 meV at the DP[42], however, the energy position of the DP with respect to the VBM of h-BN increases to 1.64 eV, $\Delta_{DP} = 1.38 \rightarrow 1.64$ eV. The projected DOS (PDOS) is characterized by the presence of VHSs, labelled as $v1$ and $c1$, at the same energy positions as those of G/h-BN. Both singularities are attributed to the electronic states at the M-point, with the former resulting from interlayer G/h-BN hybridizations and the latter from only the graphene p_z states. We find a different picture in h-BN/G/G. In this case, the energy bands of the graphene layers are characteristics of a graphene bilayer. However, the energy bands at the M-point are no longer degenerated since the stacking sequence (h-BN/G/G) is no longer mirror-symmetric, resulting in doubled VHS in $v1$ and $c1$, as shown in Fig. 1(d2)[43]. Finally, it is worth noting that the work functions (Φ) of the free-standing bilayer and trilayer systems (about 4.2 eV), for both stacking geometries, are close to that of free-standing graphene[44], and consistent with the near absence of net charge transfers between the h-BN and graphene sheets.

B. h-BN/G BLs on buffer layer/SiC(0001)

1. Energetic and electronic properties

Epitaxial graphene on SiC(0001) covered by a carbon buffer layer, here denoted as G/SiC [Fig. 8(a) (Appendix B)] has been extensively studied in the past few years. In consonance with the current literature, we find that (i) the graphene binding strength is determined by the vdW interaction, with a binding energy of 20 meV/(1×1), and (ii) there is a net charge transfer from SiC surface

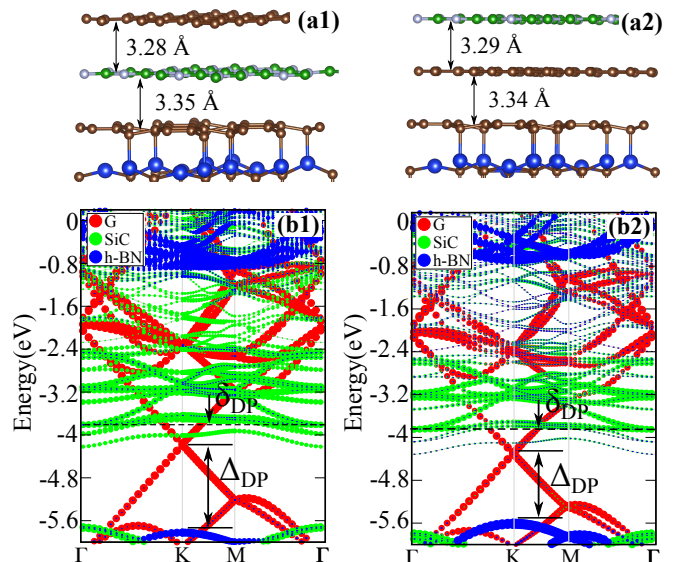


FIG. 2. Structural models of h-BN ML (a1) on-top of the G/SiC(0001) surface [h-BN/G/SiC], and (a2) encapsulated between graphene single layer and the SiC surface, [G/h-BN/SiC]. Orbital projected electronic band structure of G/h-BN/SiC(0001) (b1), and h-BN/G/SiC (b2). The electronic density of states is proportional to the size of the filled circles, with blue circles (red circles) corresponding to the projection on the boron and nitrogen (carbon) p -orbitals, and green circles to the p -orbitals of the surface Si dangling bonds. The zero energy was set at the vacuum level, and the black dotted line indicates the Fermi level.

to the upper single-layer graphene, which results in a n -type doping of graphene at about $2.3 \times 10^{13} e/cm^2$ [45–48]. Such an electron doping results in a reduction of the graphene work function compared to that of single-layer free-standing graphene, namely $\Phi = 4.17 \rightarrow 3.69$ eV.

Next, we consider heterostructures combining an h-BN/G BLs on buffer layer/SiC(0001). In Figs. 2(a1) and (a2) we show the SiC(0001) surface covered by the carbon buffer layer and an h-BN ML below (G/h-BN/SiC) and above (h-BN/G/SiC) single-layer graphene. Our total energy results indicate that the G/h-BN/SiC is energetically more stable by 36 meV/(1×1) in comparison with the latter stacking structure. The interlayer binding strength is mediated mainly by vdW interactions, with an equilibrium distance of about 3.3 Å independent of the stacking order.

In both systems, the linear energy dispersion at the K-point has been preserved, Fig. 2(b), characterized by a small energy gap at the K-point due to the lack of the A and B sublattice symmetry[49]. Moreover, it is noticeable that the energy positions of the h-BN's occupied states are downshifted in G/h-BN/SiC compared to those of h-BN/G/SiC, resulting in $\Delta_{DP} = 1.64$ and 1.29 eV, respectively, indicating that the h-BN states in G/h-BN/SiC are more tightly bonded than those in h-BN/G/SiC. Calculating the averaged orbital binding energy of the h-BN states ($\bar{\epsilon}$) allows one to see this assertion in quantitative

terms. Here $\bar{\epsilon}$ can be written as,

$$\bar{\epsilon} = \frac{\int_{-\infty}^{E_F} \epsilon g(\epsilon) d\epsilon}{\int_{-\infty}^{E_F} g(\epsilon) d\epsilon}, \quad (4)$$

where ϵ is the single-particle energy level and $g(\epsilon)$ is the respective PDOS of h-BN in G/h-BN/ and h-BN/G/SiC. We found that consistent with the energetic preference for the encapsulated h-BN, the electronic states of h-BN in G/h-BN/SiC are more tightly bonded than those in h-BN/G/SiC by 66 meV, with the out-of-plane p_z orbitals accounting for the major contribution (67%).

The charge doping through the layered systems will depend on the G and h-BN stacking orders. In Figs. 3(a) and (b) we present the net charge transfers ($\Delta\rho$) along G/h-BN/ and h-BN/G/SiC[50]. The charge transfers are ruled by the out-of-plane p_z orbitals of the graphene adlayer, h-BN, and the carbon buffer layer. In G/h-BN/SiC, we found that the n -type doping of graphene ($\Delta\rho > 0$) reduces from $\approx 2 \times 10^{13} e/cm^2$ (in G/SiC, not shown) to $0.8 \times 10^{13} e/cm^2$, followed by (ii) an electrical polarization of the h-BN layer with $\Delta\rho > 0$ (< 0) below (above) the sheet, Fig. 3(a). In this case, the intercalated h-BN sheet acts as a block layer to the SiC \rightarrow G charge transfer. Meanwhile, we found that n -type doping of graphene in h-BN/G/SiC is almost identical to that of G/SiC, namely $\Delta\rho = 1.45 \times 10^{13} e/cm^2$ in Fig. 3(b), indicating that the topmost h-BN sheet very slightly affects the charge transfer profile. Thus, despite having identical interlayer equilibrium geometries, G/h-BN/ and h-BN/G/SiC exhibit substantially distinct net charge transfers, which in its turn has an impact on the electronic band structures[44]. For instance, as shown in Figs. 2(b1) and (b2), the DP lies at $\delta_{DP} = 0.28$ and 0.32 eV below the Fermi level (E_F) in G/h-BN/ and h-BN/G/SiC, respectively, which is consistent with the lower doping rate in G/h-BN/SiC when compared with that of h-BN/G/SiC. By considering the vacuum level (E_{vac}) as the energy reference, we find the graphene DP at 4.15 and 4.27 eV below E_{vac} in G/h-BN/ and h-BN/G/SiC. It is possible to measure such difference in work function via Kelvin probe force microscopy (KPFM)[44, 51, 52]. Thus, this method can be seen as a powerful tool for identifying the stacking order of large-area G/h-BN heterostructures grown via physical- or chemical-vapor deposition[53].

In addition to the downshift of $\bar{\epsilon}$, the energetic preference for the G/h-BN/SiC system can be attributed to the differences in the net charge transfer profiles between G/h-BN/ and h-BN/G/SiC [Fig. 3]. In the former, we have a negatively charged G layer neighboring a positively charged h-BN layer, while, in the latter, we have both G and h-BN negatively charged, resulting in a lower interlayer electrostatic energy in G/h-BN/SiC when compared with that of h-BN/G/SiC. Indeed, our total results show that the classical electron-electron interaction, Hartree energy, brings the major contribution to the energetic preference of G/h-BN/SiC in comparison with the

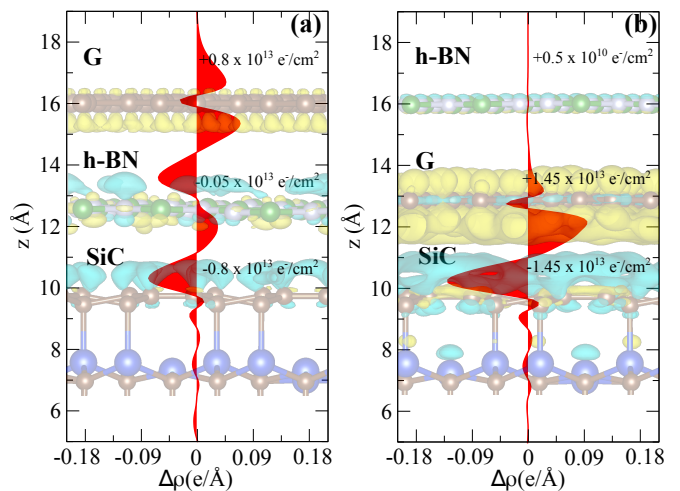


FIG. 3. Map of the electronic charge transfers [$\Delta\rho(\mathbf{r})$], and the planar averaged $\Delta\rho$ [$\Delta\rho(z)$] of the bilayer/SiC systems, G/h-BN/SiC (a), h-BN/G/SiC (b). In the background, we show the electronic charge transfer isosurface for each stacking. Here the isosurface value is $2 \times 10^{-4} e/\text{\AA}^3$. Yellow (Blue) isosurfaces indicate $\Delta\rho > 0$ (< 0)

other stacking geometries. Thus, we can infer that the net charge transfers through the G/h-BN stacked layers, upon its interaction with the SiC surface, also make an important contribution to the energetic stability of the h-BN encapsulated geometry, G/h-BN/SiC.

2. Structural characterization: XANES

In order to provide a more complete picture and connection between the stacking geometry and the electronic structure of the G/h-BN/ and h-BN/G/SiC systems, we performed a set of XANES simulations based on the first-principles DFT calculations. Initially, we examined the K-edge absorption spectra of the graphene's carbon atoms, with the light polarization vector perpendicular (ϵ_{\perp}) and parallel (ϵ_{\parallel}) to the surface. Figure 4 (solid-black lines) shows our simulated C K-edge spectra of pristine graphene, characterized by the $C-1s \rightarrow \pi^*$, and $\rightarrow \sigma^*$ transitions, at 285.8 and 292.4 eV (for ϵ_{\perp} and ϵ_{\parallel}). This results in a peak-to-peak difference [$\Delta E^{PP} = E(\sigma^*) - E(\pi^*)$] of 6.61 eV, in good agreement with the experimental measurements[54–56]. In the sequence, we calculated the absorption spectra of the graphene carbon atoms in G/h-BN/ and h-BN/G/SiC [solid-blue lines in Figs. 4(a) and (b), respectively]. In agreement with the recent experimental XANES results of h-BN on SiC(0001)[58], we find that the $C-1s \rightarrow \pi^*$, and $\rightarrow \sigma^*$ absorption features of the graphene carbon atoms have been preserved, as well as the energy difference ΔE^{PP} , supporting the vdW interactions between the G and h-BN layers[58]. When compared with pristine graphene, we found that the absorption spectra in

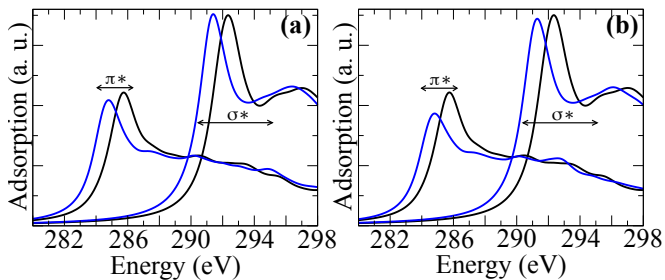


FIG. 4. Simulated C K-edge XANES of G/h-BN/SiC (a) and h-BN/G/SiC (b). The zero energy is set to the calculated highest occupied state plus the experimental C-1s binding energy.[57]

TABLE I. Graphene's C-1s core-level shift (ΔBE in eV) of G/h-BN and h-BN/G on SiC with respect to the one of free-standing graphene.

	G/h-BN/	h-BN/G/
ΔBE	-1.19	-1.02

G/h-BN/ and h-BN/G/SiC are downshifted by about 1 eV, where the C-1s $\rightarrow \sigma^*$ absorption features have been preserved. In contrast, it is noticeable that the C-1s $\rightarrow \pi^*$ spectra show distinct features in G/h-BN/ and h-BN/G/SiC. In the former, because the graphene sheet lies on the h-BN/SiC surface, the absorption feature is almost identical to that of the pristine system, whereas, in the latter, we find that the intensity of the absorption spectrum has been lowered upon the graphene's encapsulation by h-BN. These findings suggest that the stacking order of G and h-BN layers can be determined by the XANES spectra's ability to detect variations in the C-2p_z hybridizations in G/h-BN/ and h-BN/G/SiC.

C. G/h-BN/G TLs on buffer layer/SiC(0001)

1. Energetic and electronic properties

In this last subsection, we examine the structural/energetic, and electronic properties of the graphene and h-BN TL systems on buffer layer-covered SiC(0001) (trilayer/SiC), Fig. 5. We found that the energetic preference for the h-BN intercalated (encapsulated) between graphene layers G2/h-BN/G1/SiC [Fig. 5(a)] has been preserved, while the h-BN on the topmost surface layer, h-BN/G2/G1/SiC [Fig. 5(c)] is the energetically less favorable configuration by 14 meV/(1 \times 1). At the equilibrium geometry, the interlayer distances in G2/h-BN/G1/SiC are the same when compared with those of the free-standing G/h-BN/G heterostructure, 3.31 Å in Fig. 1(c1).

Figure 6(a) depicts the orbital projected electronic band structure of G2/h-BN/G1/SiC. It is possible to observe that (i) the linear energy dispersion of graphene

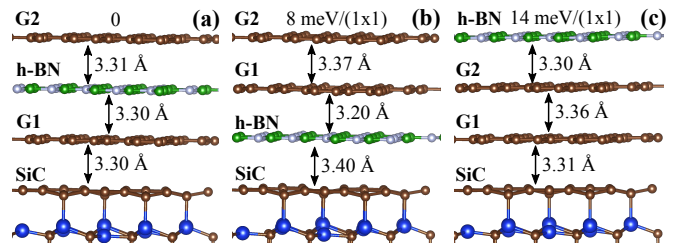


FIG. 5. Schematic models for three possible stackings of the trilayers G2, G1, and h-BN layers: (a) G2/h-BN/G1, (b) G2/G1/h-BN, and (c) h-BN/G2/G1. We also have shown the interlayer distances (in angstrom) in the figure. In addition, at the top, the total energy differences between the most stable stacking (a), which we have defined as zero energy.

TABLE II. Graphene's C-1s core-level shift (ΔBE in eV) of G2/h-BN/G1, G2/G1/h-BN, and h-BN/G2/G1 on SiC with respect to the one of free-standing graphene.

	G2/h-BN/G1/	G2/G1/h-BN/	h-BN/G2/G1/
ΔBE (G2/G1)	-1.32/ -1.49	-1.29/ -1.36	-1.39/ -1.21

has been preserved, resulting in (ii) two non-degenerated Dirac energy bands. In contrast, the electronic band structures of G2/G1/h-BN/ and h-BN/G2/G1/SiC are ruled by the formation of graphene bilayer systems, G2/G1, characterized by the emergence of parabolic bands near the Fermi level, as depicted in Figs. 9(a) and (b) Appendix C.

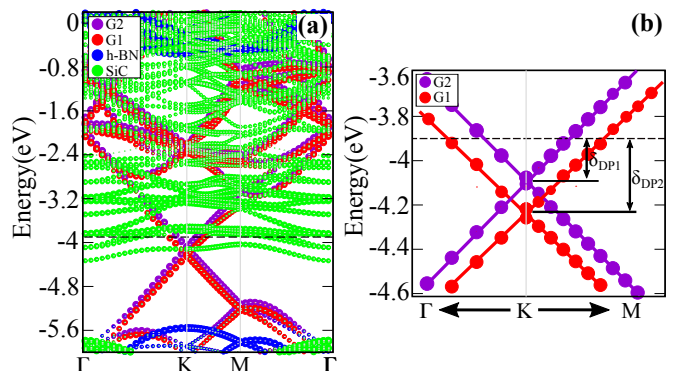


FIG. 6. (a) Projected states band structure of the single graphene layers G1-p states (red sphere) and G2-p states (purple sphere), BN-p states (blue ball) and Buffer [Si-p, C-p and H-p states] (green sphere) on G2/h-BN/G1 on the buffer. (b) Dirac cones are detailed around the Fermi level. The zero energy was set at the vacuum level, and the black dotted line indicates the Fermi level.

In G2/h-BN/G1/SiC, the Dirac points DP1 and DP2 lie below the Fermi level [Fig. 6(b)] with δ_{DP1} and δ_{DP2} of -0.18 and -0.34 eV, respectively, dictated by the charge transfers from the SiC surface to the G2/h-BN/G1 trilayer, see Fig. 7(a). Such charge transfers are mostly localized at the G1/SiC interface, resulting in a *n*-type dop-

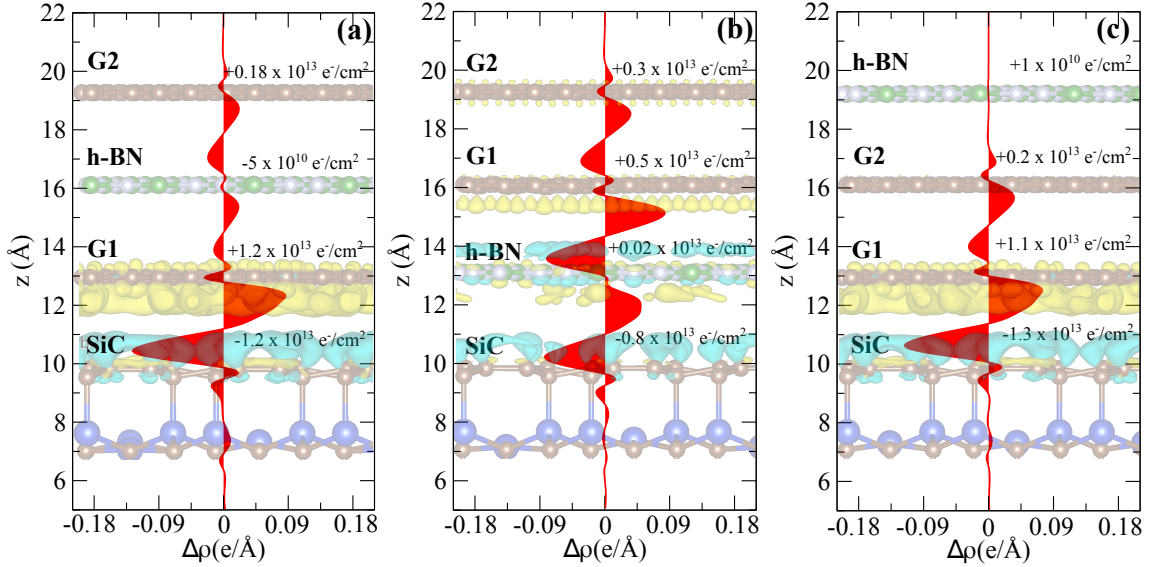


FIG. 7. Map of the electronic charge transfers $[\Delta\rho(\mathbf{r})]$, and the planar averaged $\Delta\rho$ $[\Delta\rho(z)]$ of the trilayer/SiC systems, G2/h-BN/G1/SiC (a), G2/G1/h-BN/SiC (b), and h-BN/G2/G1/SiC (c). Yellow (Blue) isosurfaces indicate $\Delta\rho > 0$ (< 0). The isosurface value is $2 \times 10^{-4} e/\text{\AA}^3$.

ing of G1 by $\Delta\rho_{G1} = 1.2 \times 10^{13} e/\text{cm}^2$, which is smaller than the doping level obtained in G/SiC, while the positive net charge density ($\Delta\rho_{\text{SiC}} = -1.2 \times 10^{13} e/\text{cm}^2$) is predominantly localized on the topmost layer of SiC. The presence of the intercalated h-BN layer decreases the electron doping of G2 to $\Delta\rho_{G2} = 0.18 \times 10^{13} e/\text{cm}^2$, while h-BN exhibits a very slight hole doping of $5 \times 10^{10} e/\text{cm}^2$.

The amount of SiC \rightarrow trilayer charge transfers are roughly the same regardless of stacking order, Fig. 7. As shown in Figs. 7(b) and (c), in the G2/G1/h-BN and h-BN/G2/G1/SiC systems, the negatively charged layers G1 and G2 are stacked in sequence, suggesting in higher electrostatic energy when compared to G2/h-BN/G1/SiC, where the negatively charged layers G1 and G2 are separated by the positively charged h-BN. Indeed, similar to what we verified in the bilayer/SiC systems, our total energy results reveal that the energetic preference of G2/h-BN/G1/SiC is dictated by the Hartree energy component. It is worth noting that in the free-standing trilayer systems [Fig. 1(c)] the energetic preference for G/h-BN/G is ruled by the electrostatic ion-ion Coulomb energy (Ewald term). In addition, further calculation of the h-BN's orbital binding energy [eq. 4] support the energetic preference for the encapsulated geometry in trilayer/SiC.

2. Structural characterization: CLS

Recent works, based X-ray photoelectron spectroscopy (XPS) experiments, have indicated the formation of sharp h-BN/G interfaces on the SiC substrate, with the absence of B clusters or the formation of chemical bonds between graphene and h-BN[7, 58]. Motivated by the re-

cent successful combination of experimental results and first-principles DFT simulations leading to an atomistic understanding of XPS spectra[33, 59, 60], here we start an investigation of the graphene's C-1s core level binding energy (BE) of the bilayer/ and trilayer/SiC systems. We focused on the dependence of the core level binding energy, i.e., the core-level shift (CLS), on G/h-BN stacking geometry and net charge transfers in bilayer/ and trilayer/SiC, Figs. 3 and 7.

We found that the graphene's C-1s core level BE reduces upon the formation of bilayer/ and trilayer/SiC systems. For instance, in G/h-BN/SiC, the SiC \rightarrow G/h-BN net charge transfers results in a reduction of the C-1s core level binding energy of 1.19 eV with respect to the one of free-standing graphene, $\Delta\text{BE} = -1.19$ eV. By changing the stacking sequence, h-BN/G/SiC, we found $\Delta\text{BE} = -1.02$ eV, thus indicating a stacking dependence of 0.17 eV in the graphene's C-1s core-level spectrum. Our results of ΔBE , summarized in Tables I and II, reveal the manifestation of two main contributions to the core-level shifts, namely (i) net charge transfer (electron doping, $\Delta\rho$), and (ii) the presence of external electric field (EEF)[61]. For instance, based on the electron doping level [(i)] of the graphene layer in h-BN/G/SiC [Fig. 3(b)], it is expected a larger reduction of the graphene's C-1s core-level BE compared with that in G/h-BN/SiC. However, this is not what we found, which can be attributed to the emergence of an EEF [(ii)] due to the positively charged layer on the SiC surface [Fig. 3(a)], which increases the BE of graphene C-1s, and thus leading to a smaller BE reduction in h-BN/G/SiC. Similarly in the trilayer/SiC system, we find that both, the electron doping [(i)], and the emergence of an EEF [(ii)], due to the trilayer/SiC interface dipole, rule the C-1s core-

level shifts, ΔBE . Further discussions of the graphene C-1s core-level shift are presented in Appendix D. It is worth noting that, despite the small energy differences ($\sim 0.1 - 0.2$ eV), our results of graphene's C-1s core-level BEs reveal a relationship between the G/h-BN stacking order and the respective CLSs.

IV. SUMMARY AND CONCLUSIONS

By means of first-principles DFT calculations, we have performed a theoretical study of G/h-BN van der Waals heterostructures on SiC(0001) covered by a carbon buffer layer. Our total energy results not only show the encapsulation of h-BN underneath epitaxial single-layer graphene in bilayer/ and trilayer/SiC systems (as inferred from recent experimental observations), but also reveal that the energetic preference for the h-BN encapsulation is ruled by a reduction of the electron-electron classical electrostatic (Hartree) energy, triggered by the electron doping of graphene. We found that the graphene layers become *n*-type doped, where the doping profile through the vdW layers is determined by the stacking geometry. Further electronic band structure calculations reveal that the linear energy band dispersion of graphene has been preserved in G/h-BN/ and G/h-BN/G/SiC systems, with the Dirac point lying below the Fermi level. Finally, we found key spectroscopic fingerprints of bilayer and trilayer SiC using K-edge X-ray absorption near edge spectroscopy (XANES) and C-1s core-level-shift (CLS) simulations, which may aid in the experimental characterization of these G/h-BN heterostructures on SiC.

ACKNOWLEDGMENTS

The authors acknowledge financial support from the Brazilian agencies CNPq, CAPES, FAPEMIG, and INCT-Nanomateriais de Carbono, and the CENAPAD-SP and Laboratório Nacional de Computação Científica (LNCC-SCAFMat2) for computer time.

Appendix A: Energetic stability of trilayers

We have performed additional calculations of the energetic stability of the trilayer systems, G/h-BN/G and h-BN/G/G, using other approaches to describe the long-range vdW interactions, namely vdW-Opt88, -OptPBE, -DF, and -TS. Our results, summarized in Table III, indeed confirm the energetic preference of the former stacking geometry, with the graphene carbon atoms aligned with the B atoms of h-BN.

TABLE III. Total energies differences (in meV/1 \times 1), of the G/h-BN/G and h-BN/G/G stacking geometries with respect to the energetically most stable configuration [G/h-BN/G with the graphene's C atom aligned with the h-BN's B atom], by using different approaches to describe the vdW interactions.

	G/h-BN/G			h-BN/G/G		
	C aling. B	C aling. N		C aling. B	C aling. N	
OptB88	0	6		5	22	
OptPBE	0	7		3	15	
DF	0	10		1	9	
TS	0	16		8	32	

Appendix B: G/SiC

Figures 8(a) and (b) show the structural model of G/SiC and electronic band structure of graphene on the SiC(0001) surface covered by a carbon buffer layer, G/SiC, respectively.

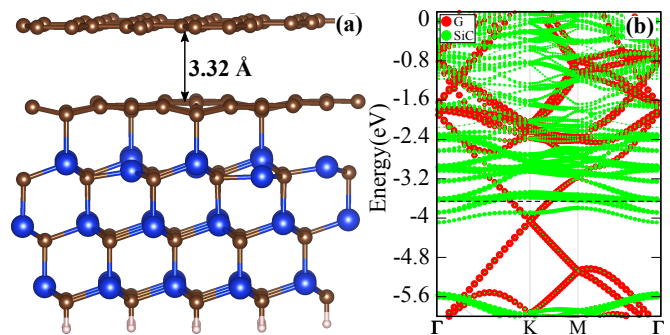


FIG. 8. Structural model (a) and the electronic band structure (b) of graphene on the SiC(0001) surface covered by a carbon buffer layer, G/SiC.

Appendix C: G₂/G₁/h-BN/ and h-BN/G₂/G₁/SiC

In Figs. 9(a) and (b) we present the orbital projected electronic band structures of the G₂/G₁/h-BN/ and h-BN/G₂/G₁/SiC systems, both characterized by the formation of massive bands below the Fermi level.

Appendix D: Core-level shifts of intermediate structures

To better comprehend the graphene's C-1s core-level shift in bilayer/ and trilayer/SiC, we calculate the BEs by considering (hypothetical) intermediate structures. For instance, in Fig. 10(a) the hypothetical structure is represented by a free-standing G/h-BN bilayer fixed at the equilibrium geometry of the G/h-BN/SiC final system. We find that BE reduces by 0.26 eV, when compared to one of the free-standing graphene, $\Delta BE = -0.26$ eV;

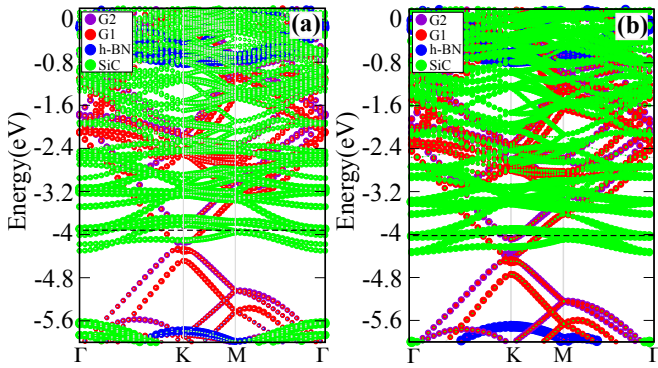


FIG. 9. Orbital projected electronic band structures of G2/G1/h-BN/SiC (a), and h-BN/G2/G1/SiC (b).

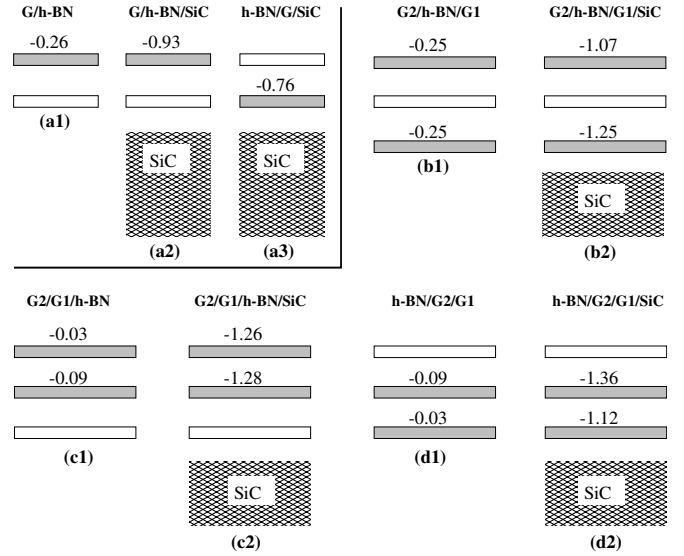


FIG. 10. Schematic diagram of the graphene's C-1s core-level shifts in the bilayer/SiC (a), and trilayer/SiC (b)-(d). (a1) Δ BE of G/h-BN with respect to the graphene monolayer, (a2) and (a3) Δ BE of G/h-BN bilayer upon its interaction with the SiC(0001) surface covered by a carbon buffer layer, SiC. (b1) Δ BE of G2/h-BN/G1 with respect to the graphene monolayer, (b2) Δ BE of G2/h-BN/G1 trilayer upon its interaction with the SiC surface. (c1) and (d1) Δ BE of G2/G1/h-BN and h-BN/G2/G1 with respect to the graphene monolayer, (c2) and (d2) Δ BE of G2/G1/h-BN and h-BN/G2/G1 trilayers upon their interaction with the SiC surface.

which can be attributed to the orbital overlap at the G/h-BN interface region.[37] As expected, we found the same result of Δ BE when we consider the equilibrium geometry of h-BN/G/SiC. In contrast, the interaction of the G/h-BN bilayer with the SiC surface (final system) results in the stacking dependent values of Δ BE, viz.: Δ BE: G/h-BN $\xrightarrow{-0.93 \text{ eV}}$ G/h-BN/SiC and Δ BE: h-BN/G $\xrightarrow{-0.76 \text{ eV}}$ h-BN/G/SiC, as schematically shown in Figs. 10(a2) and (a3). Here, we can infer that such dependence is dictated by a competition between the electron doping of graphene and the electric field due to the formation of a positively charged layer on the SiC surface, where the former (latter) reduces (increases) the BE of graphene's C-1s core-level. A similar picture has been verified in the trilayer/SiC systems, as depicted in Figs. 10(b)-(d).

* dominike@iftm.edu.br

† hiroki@ufu.br

¹ Andre K Geim and Irina V Grigorieva, "Van der waals heterostructures," Nature **499**, 419–425 (2013).

² Mathieu Massicotte, Peter Schmidt, Fabien Vialla, Kenji Watanabe, Takashi Taniguchi, Klaas-Jan Tielrooij, and Frank HL Koppens, "Photo-thermionic effect in vertical graphene heterostructures," Nature communications **7**,

12174 (2016).

³ Sarah J Haigh, Ali Gholinia, Rashid Jalil, Simon Romani, Liam Britnell, Daniel C Elias, Konstantin S Novoselov, Leonid A Ponomarenko, Andre K Geim, and R Gorbachev, "Cross-sectional imaging of individual layers and buried interfaces of graphene-based heterostructures and superlattices," Nature materials **11**, 764–767 (2012).

- ⁴ Aidan P Rooney, Aleksey Kozikov, Alexander N Rudenko, Eric Prestat, Matthew J Hamer, Freddie Withers, Yang Cao, Kostya S Novoselov, Mikhail I Katsnelson, Roman Gorbachev, *et al.*, “Observing imperfection in atomic interfaces for van der waals heterostructures,” *Nano letters* **17**, 5222–5228 (2017).
- ⁵ Atsushi Koma, Kazumasa Sunouchi, and Takao Miyajima, “Fabrication of ultrathin heterostructures with van der waals epitaxy,” *J. Vac. Sci. Technol.* **3**, 724 (1985).
- ⁶ Nathaniel Feldberg, Oleksii Klymov, Nuria Garro, Ana Cros, Nicolas Mollard, Hanako Okuno, Marion Gruart, and Bruno Daudin, “Spontaneous intercalation of ga and in bilayers during plasma-assisted molecular beam epitaxy growth of gan on graphene on sic,” *Nanotechnology* **30**, 375602 (2019).
- ⁷ M Heilmann, M Bashouti, H Riechert, and JMJ Lopes, “Defect mediated van der waals epitaxy of hexagonal boron nitride on graphene,” *2D Materials* **5**, 025004 (2018).
- ⁸ Martin Heilmann, Victor Deinhart, Abbes Tahraoui, Katja Höflich, and J Marcelo J Lopes, “Spatially controlled epitaxial growth of 2d heterostructures via defect engineering using a focused he ion beam,” *npj 2D Materials and Applications* **5**, 1–7 (2021).
- ⁹ Shengnan Wang, Jack Crowther, Hiroyuki Kageshima, Hiroki Hibino, and Yoshitaka Taniyasu, “Epitaxial intercalation growth of scalable hexagonal boron nitride/graphene bilayer moiré materials with highly convergent interlayer angles,” *Acs Nano* **15**, 14384–14393 (2021).
- ¹⁰ Yang Yang, Qiang Fu, Haobo Li, Mingming Wei, Jianping Xiao, Wei Wei, and Xinhe Bao, “Creating a nanospace under an h-bn cover for adlayer growth on nickel (111),” *ACS nano* **9**, 11589 (2015).
- ¹¹ Zakaria Y Al Balushi, Ke Wang, Ram Krishna Ghosh, Rafael A Vilá, Sarah M Eichfeld, Joshua D Caldwell, Xiaoye Qin, Yu-Chuan Lin, Paul A DeSario, Greg Stone, *et al.*, “Two-dimensional gallium nitride realized via graphene encapsulation,” *Nature materials* **15**, 1166–1171 (2016).
- ¹² Woojoo Lee, Yuanxi Wang, Wei Qin, Hyunsue Kim, Mengke Liu, T Nathan Nunley, Bin Fang, Rinu Maniyara, Chengye Dong, Joshua A Robinson, *et al.*, “Confined monolayer ag as a large gap 2d semiconductor and its momentum resolved excited states,” *Nano letters* **22**, 7841–7847 (2022).
- ¹³ Furkan Turker, Chengye Dong, Maxwell T Wetherington, Hesham El-Sherif, Stephen Holoviak, Zachary J Trdinich, Eric T Lawson, Gopi Krishnan, Caleb Whittier, Susan B Sinnott, *et al.*, “2d oxides realized via confinement heteroepitaxy,” *Advanced Functional Materials* **33**, 2210404 (2023).
- ¹⁴ J. P. Perdew, K. Burke, and M. Ernzerhof, *Phys. Rev. Lett.* **77**, 3865 (1996).
- ¹⁵ P. E. Blüchl, *Phys. Rev. B* **50**, 17953 (1994).
- ¹⁶ G. Kresse and J. Furthmüller, *Comput. Mater. Sci.* **6**, 15 (1996).
- ¹⁷ G. Kresse and J. Furthmüller, *Phys. Rev. B* **54**, 11169 (1996).
- ¹⁸ A. Tkatchenko and M. Scheffler, *Phys. Rev. Lett.* **102**, 073005 (2009).
- ¹⁹ H. J. Monkhorst and J. D. Pack, *Phys. Rev. B* **13**, 5188 (1976).
- ²⁰ Guohong Li, A. Luican, J. M. B. Lopes dos Santos, A. H. Castro Neto, A. Reina, J. Kong, and E. Y. Andrei, “Observation of van hove singularities in twisted graphene layers,” *Nature Physics* **6**, 109–113 (2010).
- ²¹ O. Pankratov, S. Hensel, and M. Bockstedte, “Electron spectrum of epitaxial graphene monolayers,” *Phys. Rev. B* **82**, 121416 (2010).
- ²² J.E. Padilha, R.B. Pontes, F. Crasto de Lima, R. Kagimura, and R.H. Miwa, “Graphene on the oxidized sic surface and the impact of the metal intercalation,” *Carbon* **145**, 603–613 (2019).
- ²³ Oana Bunău and Matteo Calandra, “Projector augmented wave calculation of x-ray absorption spectra at the l 2, 3 edges,” *Physical Review B* **87**, 205105 (2013).
- ²⁴ Christos Gougoussis, Matteo Calandra, Ari P. Seitsonen, and Francesco Mauri, “First-principles calculations of x-ray absorption in a scheme based on ultrasoft pseudopotentials: From α -quartz to high- T_c compounds,” *Phys. Rev. B* **80**, 075102 (2009).
- ²⁵ Mathieu Taillefumier, Delphine Cabaret, Anne-Marie Flank, and Francesco Mauri, “X-ray absorption near-edge structure calculations with the pseudopotentials: Application to the k edge in diamond and α -quartz,” *Physical Review B* **66**, 195107 (2002).
- ²⁶ P. Giannozzi *et al.*, *J. Phys.: Condens. Matter* **21**, 395502 (2009).
- ²⁷ Chris J Pickard and Francesco Mauri, “All-electron magnetic response with pseudopotentials: Nmr chemical shifts,” *Physical Review B* **63**, 245101 (2001).
- ²⁸ Laura Bianchettin, Alessandro Baraldi, Stefano de Gironcoli, Silvano Lizzit, Luca Petaccia, Erik Vesselli, Giovanni Comelli, and Renzo Rosei, “Geometric and electronic structure of the nrh(100) system by core-level photoelectron spectroscopy: Experiment and theory,” *Phys. Rev. B* **74**, 045430 (2006).
- ²⁹ Oksana Plekan, Vitaliy Feyer, Robert Richter, Marcello Coreno, Monica de Simone, Kevin C. Prince, and Vincenzo Carravetta, “Investigation of the amino acids glycine, proline, and methionine by photoemission spectroscopy,” *The Journal of Physical Chemistry A* **111**, 10998–11005 (2007).
- ³⁰ E. Pehlke and M. Scheffler, “Evidence for site-sensitive screening of core holes at the si and ge (001) surface,” *Phys. Rev. Lett.* **71**, 2338–2341 (1993).
- ³¹ P Bolognesi, G Mattioli, P O’Keeffe, V Feyer, O Plekan, Y Ovcharenko, KC Prince, M Coreno, A Amore Bonapasta, and L Avaldi, “Investigation of halogenated pyrimidines by x-ray photoemission spectroscopy and theoretical dft methods,” *The Journal of Physical Chemistry A* **113**, 13593–13600 (2009).
- ³² Flaminia Rondino, Daniele Catone, Giuseppe Mattioli, Aldo Amore Bonapasta, Paola Bolognesi, Anna Rita Casavola, Marcello Coreno, Patrick O’Keeffe, and Lorenzo Avaldi, “Competition between electron-donor and electron-acceptor substituents in nitrotoluene isomers: a photoelectron spectroscopy and ab initio investigation,” *RSC Adv.* **4**, 5272–5282 (2014).
- ³³ MC Castrovilli, P Bolognesi, E Bodo, G Mattioli, A Cartoni, and L Avaldi, “An experimental and theoretical investigation of xps and nexafs of 5-halouracils,” *Physical Chemistry Chemical Physics* **20**, 6657–6667 (2018).
- ³⁴ R Larciprete, A Goldoni, A Grošo, S Lizzit, and G Paolucci, “The photochemistry of ch4 adsorbed on pt (1 1 1) studied by high resolution fast xps,” *Surface science* **482**, 134–140 (2001).
- ³⁵ Camilla Coletti, Konstantin V Emtsev, Alexei A Zakharov, Thierry Ouisse, Didier Chaussende, and Ulrich Starke,

- “Large area quasi-free standing monolayer graphene on 3c-sic (111),” *Applied Physics Letters* **99**, 081904 (2011).
- ³⁶ Gianluca Giovannetti, Petr A Khomyakov, Geert Brocks, Paul J Kelly, and Jeroen Van Den Brink, “Substrate-induced band gap in graphene on hexagonal boron nitride: Ab initio density functional calculations,” *Physical Review B* **76**, 073103 (2007).
- ³⁷ Yingcai Fan, Mingwen Zhao, Zhenhai Wang, Xuejuan Zhang, and Hongyu Zhang, “Tunable electronic structures of graphene/boron nitride heterobilayers,” *Applied Physics Letters* **98**, 083103 (2011).
- ³⁸ Soo Min Kim, Allen Hsu, PT Araujo, Yi-Hsien Lee, Tomas Palacios, Mildred Dresselhaus, Juan-Carlos Idrobo, Ki Kang Kim, and Jing Kong, “Synthesis of patched or stacked graphene and hbn flakes: a route to hybrid structure discovery,” *Nano letters* **13**, 933–941 (2013).
- ³⁹ Minghu Pan, Liangbo Liang, Wenzhi Lin, Soo Min Kim, Qing Li, Jing Kong, Mildred S Dresselhaus, and Vincent Meunier, “Modification of the electronic properties of hexagonal boron-nitride in bn/graphene vertical heterostructures,” *2D Materials* **3**, 045002 (2016).
- ⁴⁰ Jingang Wang, Fengcai Ma, and Mengtao Sun, “Graphene, hexagonal boron nitride, and their heterostructures: properties and applications,” *RSC advances* **7**, 16801–16822 (2017).
- ⁴¹ DI Indolese, R Delagrance, P Makk, JR Wallbank, K Wanatabe, T Taniguchi, and C Schönenberger, “Signatures of van hove singularities probed by the supercurrent in a graphene-hbn superlattice,” *Physical review letters* **121**, 137701 (2018).
- ⁴² Raúl M Torres-Rojas, David A Contreras-Solorio, Luis Hernández, and Agustín Enciso, “Band gap variation in bi, tri and few-layered 2d graphene/hbn heterostructures,” *Solid State Communications* **341**, 114553 (2022).
- ⁴³ Ashwin Ramasubramaniam, Doron Naveh, and Elias Towe, “Tunable band gaps in bilayer graphene- bn heterostructures,” *Nano letters* **11**, 1070–1075 (2011).
- ⁴⁴ Samir Mammadov, Jürgen Ristein, Julia Krone, Christian Raidel, Martina Wanke, Veit Wiesmann, Florian Speck, and Thomas Seyller, “Work function of graphene multilayers on sic (0001),” *2D Materials* **4**, 015043 (2017).
- ⁴⁵ Alexander Mattausch and Oleg Pankratov, “Ab initio study of graphene on sic,” *Physical Review Letters* **99**, 076802 (2007).
- ⁴⁶ F. Varchon, R. Feng, J. Hass, X. Li, B. Ngoc Nguyen, C. Naud, P. Mallet, J.-Y. Veuillen, C. Berger, E. H. Conrad, and L. Magaud, *Phys. Rev. Lett.* **99**, 126805 (2007).
- ⁴⁷ O. Pankratov, S. Hensel, P. Götzfried, and M. Bockstedte, *Phys. Rev. B* **86**, 155432 (2012).
- ⁴⁸ Gabriele Scლაუzero and Alfredo Pasquarello, *Phys. Rev. B* **85**, 161405(R) (2012).
- ⁴⁹ S. Y. Zhou, G.-H. Gweon, A. V. Fedorov, P. N. First, W. A. DE Heer, D.-H. Lee F. Guinea, A. H. Castro Neto, and A. Lamzara, *Nature Material*. **6**, 770 (2007).
- ⁵⁰ Here we have defined $\Delta\rho$ as $\rho_{G/h-BN/SiC} - (\rho_{G/h-BN} + \rho_{SiC})$ in G/h-BN/SiC, and $\rho_{h-BN/G/SiC} - (\rho_{h-BN/G} + \rho_{SiC})$ in h-BN/G/SiC.
- ⁵¹ Young-Jun Yu, Yue Zhao, Sunmin Ryu, Louis E Brus, Kwang S Kim, and Philip Kim, “Tuning the graphene work function by electric field effect,” *Nano letters* **9**, 3430–3434 (2009).
- ⁵² Ivan Shtepliuk, Tihomir Iakimov, Volodymyr Khraunovskyy, Jens Eriksson, Filippo Giannazzo, and Rositsa Yakimova, “Role of the potential barrier in the electrical performance of the graphene/sic interface,” *Crystals* **7**, 162 (2017).
- ⁵³ J Marcelo J Lopes, “Synthesis of hexagonal boron nitride: From bulk crystals to atomically thin films,” *Progress in Crystal Growth and Characterization of Materials* **67**, 100522 (2021).
- ⁵⁴ Theanne Schiros, Dennis Nordlund, Lucia Palova, Deborah Prezzi, Liuyan Zhao, Keun Soo Kim, Ulrich Wurstbauer, Christopher Gutierrez, Dean Delongchamp, Chernoy Jaye, *et al.*, “Connecting dopant bond type with electronic structure in n-doped graphene,” *Nano letters* **12**, 4025–4031 (2012).
- ⁵⁵ Abdelkarim Ouerghi, Mathieu G Silly, Massimiliano Marangolo, Claire Mathieu, Mahmoud Eddrief, Matthieu Picher, Fausto Sirotti, Souliman El Moussaoui, and Rachid Belkhou, “Large-area and high-quality epitaxial graphene on off-axis sic wafers,” *Acs Nano* **6**, 6075–6082 (2012).
- ⁵⁶ Andreas Lippitz, Jörg F Friedrich, and Wolfgang ES Unger, “Plasma bromination of hopg surfaces: A nexafs and synchrotron xps study,” *Surface science* **611**, L1–L7 (2013).
- ⁵⁷ Grzegorz Greczynski and Lars Hultman, “X-ray photoelectron spectroscopy: towards reliable binding energy referencing,” *Progress in Materials Science* **107**, 100591 (2020).
- ⁵⁸ Haikel Sediri, Debora Pierucci, Mahdi Hajlaoui, Hugo Henck, Gilles Patriarche, Yannick J Dappe, Sheng Yuan, Bérangère Toury, Rachid Belkhou, Mathieu G Silly, *et al.*, “Atomically sharp interface in an h-bn-epitaxial graphene van der waals heterostructure,” *Scientific reports* **5**, 1–10 (2015).
- ⁵⁹ Aldo Ugolotti, Shashank S Hariviyasi, Anu Baby, Marcos Dominguez, Anna Lisa Pinardi, Maria Francisca Lopez, Jose Angel Martin-Gago, Guido Fratesi, Luca Floreano, and Gian Paolo Brivio, “Chemisorption of pentacene on pt (111) with a little molecular distortion,” *The Journal of Physical Chemistry C* **121**, 22797–22805 (2017).
- ⁶⁰ Dorothea Golze, Markus Hirvensalo, Patricia Hernández-León, Anja Aarva, Jarkko Etula, Toma Susi, Patrick Rinke, Tomi Laurila, and Miguel A Caro, “Accurate computational prediction of core-electron binding energies in carbon-based materials: A machine-learning model combining density-functional theory and gw,” *Chemistry of Materials* **34**, 6240–6254 (2022).
- ⁶¹ Paul S Bagus, Francesc Illas, Gianfranco Pacchioni, and Fulvio Parmigiani, “Mechanisms responsible for chemical shifts of core-level binding energies and their relationship to chemical bonding,” *Journal of electron spectroscopy and related phenomena* **100**, 215–236 (1999).